JGR Oceans

RESEARCH ARTICLE
10.1029/2021JC018276

Contributions of Different Sea-Level Processes to High-Tide Flooding Along the U.S. Coastline

S. Li[1,2], T. Wahl[2], A. Barroso[2], S. Coats[3], S. Dangendorf[4], C. Piecuch[5], Q. Sun[4], P. Thompson[6], and L. Liu[1]

[1]State Key Laboratory of Geodesy and Earth's Dynamics, Innovation Academy for Precision Measurement Science and Technology, Chinese Academy of Sciences, Wuhan, China, [2]Department of Civil, Environmental and Construction Engineering and National Center for Integrated Coastal Research, University of Central Florida, Orlando, FL, USA, [3]Department of Earth Sciences, University of Hawai'i, Honolulu, HI, USA, [4]Department of River-Coastal Science and Engineering, Tulane University, New Orleans, LA, USA, [5]Department of Physical Oceanography, Woods Hole Oceanographic Institution, Woods Hole, MA, USA, [6]Department of Oceanography, University of Hawai'i, Honolulu, HI, USA

Key Points:

- A novel water level decomposition method is used to develop a database of the contributions of different sea level processes to water levels
- Fewer sea level components can combine to push water levels above high-tide flooding (HTF) thresholds due to sea-level rise
- Co-variability between sea-level components leads to compounding effects causing additional (or fewer) HTF events

Supporting Information:

Supporting Information may be found in the online version of this article.

Correspondence to:

T. Wahl and L. Liu,
t.wahl@ucf.edu;
llt@asch.whigg.ac.cn

Citation:

Li, S., Wahl, T., Barroso, A., Coats, S., Dangendorf, S., Piecuch, C., et al. (2022). Contributions of different sea-level processes to high-tide flooding along the U.S. coastline. *Journal of Geophysical Research: Oceans*, *127*, e2021JC018276. https://doi.org/10.1029/2021JC018276

Received 24 NOV 2021
Accepted 2 JUN 2022

Abstract Coastal communities across the United States (U.S.) are experiencing an increase in the frequency of high-tide flooding (HTF). This increase is mainly due to sea-level rise (SLR), but other factors such as intra- to inter-annual mean sea level variability, tidal anomalies, and non-tidal residuals also contribute to HTF events. Here we introduce a novel decomposition approach to develop and then analyze a new database of different sea-level components. Those components represent processes that act on various timescales to contribute to HTF along the U.S. coastline. We find that the relative importance of components to HTF events strongly varies in space and time. Tidal anomalies contribute the most along the west and northeast coasts, where HTF events mostly occur in winter. Non-tidal residuals are most important along the Gulf of Mexico and mid-Atlantic coasts, where HTF events mostly occur in fall. We also quantify the minimum number of components that were required to cause HTF events in the past and how this number changed over time. The results highlight that at present, due to SLR, fewer components are needed to combine to push water levels above HTF thresholds, but tidal anomalies alone are still not sufficient to reach HTF thresholds in most locations. Finally, we explore how co-variability between different components leads to compounding effects. In some places, positive correlation between sea-level components leads to significantly more HTF events than would be expected if sea-level components were uncorrelated, whereas in other places negative correlation leads to fewer HTF events.

Plain Language Summary High-tide flooding, also known as nuisance flooding or minor flooding, is one of the most obvious outcomes of climate change and associated sea-level rise (SLR). The increased frequency of high-tide flooding (HTF) and the fact that more and more communities are affected by it, has raised public awareness. We develop a new database consisting of different sea-level components, representing different processes, and analyze their contribution to HTF. We find, for example, that ocean tides are the main driver for HTF along the U.S. west coast, while surges are relatively more important along the east coast. Due to SLR, fewer sea level components can combine to lead to HTF at present-day compared to the past. Correlation between the different sea-level components also causes compounding effects leading to more (or fewer) HTF events in certain locations. The new database and analysis that is presented here advance our understanding of the role of different sea-level processes in causing HTF along the U.S. coastline.

1. Introduction

The frequency of flooding events related to coastal sea level, ranging from minor to major, has increased over recent decades (Dahl et al., 2017; Ezer, 2019; Kulp & Strauss, 2019; Moftakhari et al., 2015; Moftakhari et al., 2017; Sweet & Park, 2014; Sweet. et al., 2018) and will continue to increase in the future (Ray & Foster, 2016; Thompson et al., 2019, 2021; Vousdoukas et al., 2017). High-tide flooding (HTF) refers to occasions where water levels exceed pre-defined thresholds, which usually occur at high tide and are often (but not always) tied to impacts, including road closures, unsafe driving conditions, public health concerns (due to ponded flood water and sewage system surcharges), property damage, disruption of business, or degradation of infrastructure (Cherqui et al., 2015; Hino et al., 2019; Sweet & Park, 2014). Our focus in this analysis is on the minor flooding threshold as defined in Sweet et al. (2018). Future sea-level rise (SLR) will not just increase the frequency of HTF events but also their duration (Moftakhari et al., 2015; Sweet. et al., 2018; Thompson et al., 2021), and conditions

that currently lead to the exceedance of the minor flood threshold are likely to lead to the exceedance of the moderate flood threshold (with more severe impacts) over the next few decades (Dahl et al., 2017).

Other terms have been used to describe HTF including nuisance flooding, minor flooding, or sunny-day flooding. Here we follow the terminology used by Sweet et al. (2018) and Thompson et al. (2021), among others, in using the term HTF. Importantly, HTF does not imply that high tides alone are responsible for pushing water levels above flooding thresholds Instead, it is often a combination of different sea-level processes which combined lead to HTF, but the thresholds are often exceeded around high tide (especially in places with large tidal ranges).

The effect of SLR on HTF frequencies has been studied in detail (e.g., Dahl et al., 2017; Moftakhari et al., 2015; Taherkhani et al., 2020; Vitousek et al., 2017), while the relationship between HTF and other sea level processes (acting on various time scales) had less attention. Li et al. (2021), for example, showed that amplified tides also contributed to the observed increase in the frequency of HTF along the U.S. coastline, in particular in urbanized estuaries. The role of other sea level processes, such as the mean sea level (MSL) cycle, non-tidal residuals, or waves, in creating high coastal water levels has been studied for example, in Venice (Ferrarin et al., 2022), Latin America and the Caribbean (Losada et al., 2013), Australia (Hague et al., 2022; Lowe et al., 2021), the U.S. west coast (Serafin et al., 2017), and globally (Melet et al., 2018; Merrifield et al., 2013; Rueda et al., 2017); but none of these previous studies specifically focused on HTF and also often assumed stationarity in certain sea level processes. Here we build on these previous assessments to investigate the role of different sea level processes in generating HTF events and how this has changed over time. We use time series analysis to decompose hourly still water level observations (i.e., dynamic wave contributions are not accounted for) from 120 tide gauges into five components representing distinct processes. The decomposition is performed based on time scale and leads to hourly time series of (a) SLR, representing a non-linear long-term trend in MSL; (b) interannual-to-decadal MSL variability (ID); (c) the seasonal MSL cycle (SC) with varying amplitudes and phase lags over time (Wahl et al., 2014); (d) tidal anomaly (TA), representing sub-daily to decadal variations in tides including possible long-term changes in tidal range; and (e) NTR, representing mainly high frequency variability related to weather but also lower-frequency variability associated with other phenomena at sub-seasonal time scales. SLR is the main driver for the observed and projected increase in HTF but alone does not create HTF events. One or more of the sea-level components outlined above need to superimpose on SLR and these components can also change over time, contributing more or less to HTF events during certain time periods (see e.g., Wahl et al. (2014) and Calafat et al. (2018) for and Li et al. (2021) for TA, or Wahl and Chambers (2015) and Rashid et al. (2019) for NTR).

We develop and use the new database of sea-level components to address four scientific objectives. First, we identify the spatial and temporal variability of the contributions of different sea-level components (or processes) to still water levels that resulted in HTF since 1950. Second, we quantify how many components were required to create HTF, how this has changed over time, and the associated HTF durations. Third, we explore the seasonal variability in the contribution of different sea-level components to still water levels which caused HTF. Finally, we assess the co-variability between different sea-level components and how these lead to (positive or negative) compounding effects.

2. Data

We use hourly and monthly sea level data from coastal tide gauges retrieved from the National Oceanic and Atmospheric Administration (NOAA) Tides and Currents website (https://tidesandcurrents.noaa/gov/map/index.shtml). We only consider records that have hourly data for more than 20 years, resulting in 120 tide gauges that are analyzed. We also use annual sea level data for the same tide gauges obtained from the Permanent Service for Mean Sea Level https://www.psmsl.org/ along with datum information to ensure consistency between the hourly/monthly and annual data.

HTF thresholds defined by the National Weather Service (NWS) were taken from Sweet et al. (2018) complemented by NOAA (2022) (https://api.tidesandcurrents.noaa.gov/mdapi/prod/webapi/stations/8447930/floodlevels.json?units=metric), providing official and locally relevant HTF thresholds at 93 out of the 120 tide gauges analyzed here. For locations where NWS flooding thresholds are not available, they were inferred using the following regression function (Sweet et al., 2018):

$$y = 1.04x + 0.5 \quad (1)$$

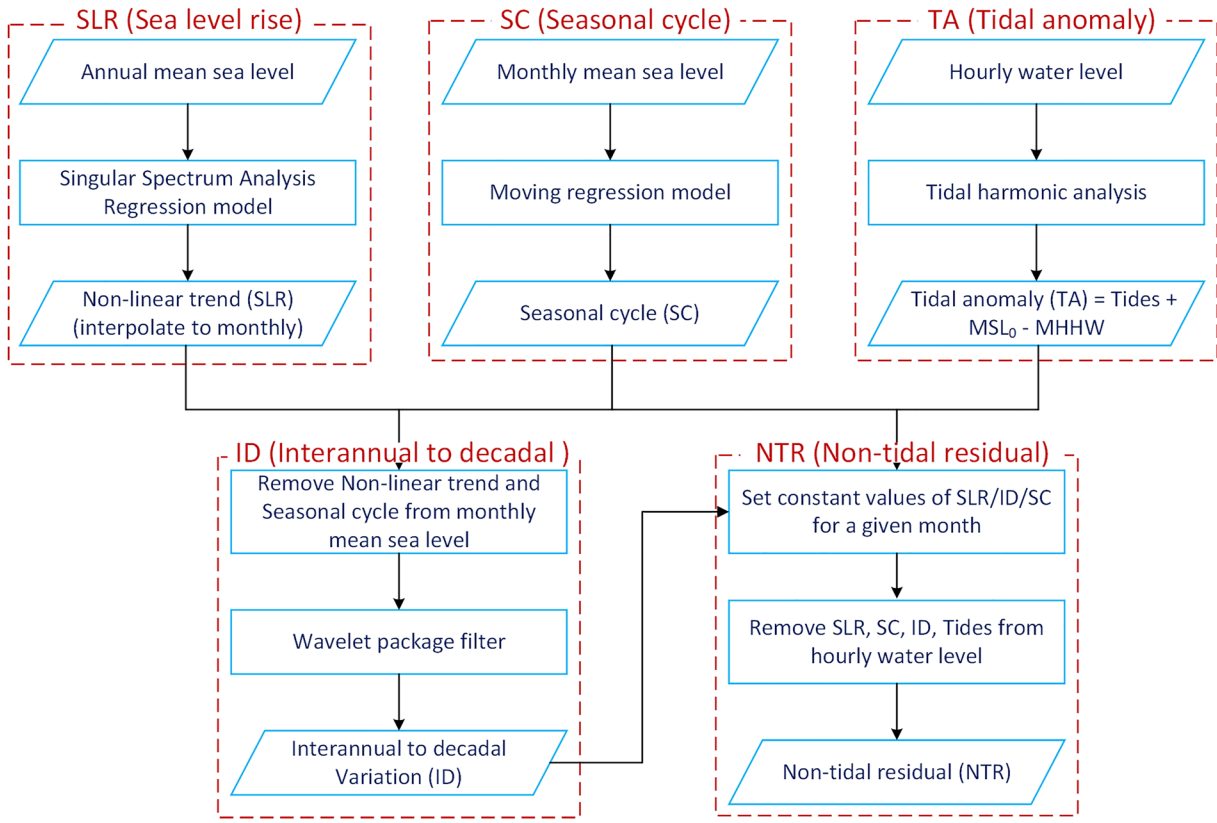

Figure 1. Flowchart of the water level decomposition process to derive sea-level rise (SLR), Seasonal cycle (SC), tidal anomaly (TA), interannual-to-decadal (ID) and Non-tidal residual (NTR). Rectangles represent analysis steps and parallelograms represent data input and output.

where x is the diurnal range (i.e., the difference between Mean Higher High Water (MHHW) and mean lower low water (MLLW)) and y is the HTF threshold above MLLW (in meters).

3. Methods

3.1. Water Level Decomposition

Here we outline the different analytical steps taken, and methods used, to derive the different sea level components (see Figure 1 and Table 1). The following Section 3.2 outlines how some of these methodological choices affect the results.

Table 1
Definition of Sea Level Components

Component	Abbreviation	Definition	References
Non-linear trend	SLR	Non-linear trend with periods >30 years (quadratic fit for time series shorter than 30 years)	Wahl et al. (2013); Dangendorf et al. (2017)
Interannual to decadal variations	ID	Interannual to decadal variations with periods >1 year and <30 years	Calafat et al. (2012); Dangendorf et al. (2014)
Seasonal cycle	SC	Seasonal cycle comprised of annual and semi-annual component	Wahl et al. (2014)
Tides	TA	Predicted tide level plus MSL_0 relative to MHHW	Pawlowicz et al. (2002)
Non-tidal residual	NTR	Non-tidal residual after removing SLR, ID, SC and TA from observed water levels	Pugh and Woodworth (2014)

The relative SLR component is obtained by applying singular spectrum analysis (SSA) to annual MSL time series at sites with records longer than 30 years. We use an embedding dimension of 15 (corresponding to a cutoff period of 30 years) accompanied by a Monte-Carlo autoregressive padding approach for adaptive smoothing near the time series boundaries; this methodology copes with edge effects and was applied similarly in previous assessments of long-term non-linear SLR (e.g., Dangendorf et al., 2017; Wahl et al., 2013). For records with data lengths between 20 and 30 years, we use quadratic least squares fit to annual MSL data to derive the SLR component. Note that using a 30 year cutoff to derive the SLR component does not mean that it only includes anthropogenic SLR, as it will also include long-term variability/periodicity (e.g., Chambers et al., 2012). Annual data is then linearly interpolated to monthly data and hourly values are derived by assuming constant values in each month.

The SC component, reflecting the seasonal mean level cycle, is obtained next by fitting harmonics to observed monthly MSL data as follows:

$$Z_0(t) = \underline{Z}_0 + \mathrm{at} + A_1 \cos\cos\left[\frac{2\pi}{12}(t-\Phi_1)\right] + A_2 \cos\cos\left[\frac{2\pi}{6}(t-\Phi_2)\right] \quad (2)$$

Where $\underline{Z}_0$ is a constant value, a is a linear trend, A_1 and A_2 the amplitudes of the annual and semi-annual cycles, Φ_1 and Φ_2 the phases of the annual and semi-annual cycles, and t the time in months. Following previous studies (e.g., Wahl et al., 2014) the least squares fit is applied to running 5 year windows of the monthly MSL time series, shifted by 1 month at each time step. Inter-annual variability can lead to trends within individual 5 year windows, therefore the linear trend component a is included in Equation 1 (note, that if we first removed SLR would the SC results would not change). Around data gaps, values are calculated when at least 3 years of data are available. Hourly values are derived by assuming constant values for a given month.

The TA component is derived through a year-by-year harmonic analysis, excluding the seasonal components. The UTide Matlab package is applied to the observed hourly water level measurements (Codiga, 2011). This procedure allows for the tidal constituents to change over time. Calendar years with less than 75% of data completeness are omitted, which can lead to gaps in the time series of the TA and NTR components. The Huber function (Fox & Weisberg, 2011; Huber, 1981), which is more robust against outliers, is applied to reduce the influence of extreme water levels on the tidal analysis. The predicted tides are then added to the base MSL, and the TA component is expressed as the difference between the resulting time series and local MHHW. Base MSL is the average hourly water level and MHHW is the average daily higher high water, both over the National Tidal Datum Epoch (1983–2001). To derive the interannual-to-decadal (ID) component, we use the wavelet packet for multiscale time series (The MathWorks, 2021b) with monthly MSL data, after the SLR and SC components have been removed (see Figure 1). We identify variations in the frequency band of 1–30 years as interannual to decadal variability. Daubechies wavelet (Daubechies, 1992), belonging to the family of orthogonal wavelets, with a decomposition level of 12 and an order of 45 (controlling the frequency resolution) was used to derive the ID component. Hourly ID values are derived by assuming constant values for a given month.

Finally, the NTR component, reflecting non-tidal residuals, is obtained by subtracting the predicted tides from the harmonic analysis from the hourly water level time series, after SLR, ID, and SC components were already removed (see Figure 1).

Table 1 one summarizes how the different water level components are defined and points to past assessments where similar definitions as the ones applied here were used for the respective components. In the following section we test how some of these definitions and methodological choices that we made for the decomposition process affect the overall results.

3.2. Sensitivity Analysis

We perform a sensitivity analysis, using the San Francisco tide gauge as an example, to evaluate how certain subjective choices made in our experiment setup to decompose observed water level time series affect the overall results and conclusions presented here. First, we compare how the SLR component changes when we use the wavelet packet to derive it instead of SSA. Differences between these two methods are small (Figure S1a in Supporting Information S1), except at the beginning and end of the records, where the SSA is combined with

autoregressive padding leading to an adaptive fit, while the wavelet analysis does not directly address these edge effects.

For the wavelet analysis to derive the ID component, we choose Daubechies wavelet with an order of 45, which affects the frequency band division. The differences in the root mean square error (RMSE) between the resulting time series and those derived when using other orders (i.e., 15–35) are around 2–5 mm (Table S1 in Supporting Information S1, Test-A results). We also chose 12 levels for the wavelet decomposition. Using more levels leads to higher computational cost, and the sensitivity analysis shows that the differences in RMSE between the time series derived with 12 levels and those derived when using different levels (11–14) are <1 mm (Table S1 in Supporting Information S1, Test-B results). Finally, we compare results when using different frequency cutoffs (cutoffs around 1 and 30 years) in the wavelet analysis and the RMSE changes by ∼1 mm (Table S1 in Supporting Information S1, Test-C results).

We also use the Markov chain Monte Carlo method outlined in Calafat et al. (2018) to compare the differences in the SC estimate compared to the simpler regression model we implemented here. Results between the two methods are similar for the annual cycle (Figure S1c in Supporting Information S1) but differences of 1–2 cm can emerge in the semi-annual cycle estimate (Figure S1b in Supporting Information S1).

Overall, the sensitivity analysis reveals that making different choices in the experiment design can lead to slight differences in some of the absolute numbers presented here. However, we the differences are small enough to conclude that our results are robust in this sense, and that similar conclusions are reached from a variety of different methodological approaches, which gives confidence in the meaningfulness of our findings.

3.3. Assessing the Number of Components Required to Cause HTF

We are interested in identifying how many of the sea level components were required in the past to superimpose onto SLR to reach HTF thresholds (note that some events may also exceed the moderate or major flood thresholds but are not treated separately in our analysis). We combine SLR with MHHW (relative to station datum) and for all past HTF days we count how many of the other four components (TA, SC, ID, and NTR) were needed on top of SLR to cross the HTF threshold. Our interest is in identifying the minimum number of components required to cross the threshold and given that interest components with the largest contribution are counted first. If our interest was different, for example, separating the contribution of deterministic and stochastic components, a different counting procedure could be more suitable. Here, if one component alone is enough to cross the threshold (regardless of which component i.e.,) it is designated as an HTF hour where only one component is needed. If one component is not enough, the next largest component is included, and it is again tested if the threshold is exceeded, and so on. We aggregate the results for each year and show the median and the 5th and 95th percentile values. Using the same process, we also obtain information on the durations of HTF events and how long they would have lasted had they been caused by the minimum number of components. We also assess how often each component was involved, alone or in combination with others, to cause threshold exceedances. For example, when two components were required, the potential combinations would be TA + NTR, TA + ID, TA + SC, NTR + SC, NTR + ID and SC + ID. We derive the frequency of each component irrespective of the combination where it is included. We extend the same analysis to cases where three and four components were required.

3.4. Seasonal Variability in Contributions of Sea-Level Components to HTF

We first separate HTF into four seasons: Winter (December-February), Spring (March-May), Summer (June-August) and Fall (September-November). Then we aggregate HTF hours caused by different numbers of sea-level components for each season. Using the same methodology as outlined in Section. 3.2, we also explore how often each component was involved in creating a threshold exceedance.

3.5. Role of Co-Variability Between Sea-Level Components

We use phase scrambling (Prichard & Theiler, 1994) to create surrogate data sets where auto-correlations of each of the components are mimicked but cross-correlations between them are removed with the exception of those that are produced by random chance.

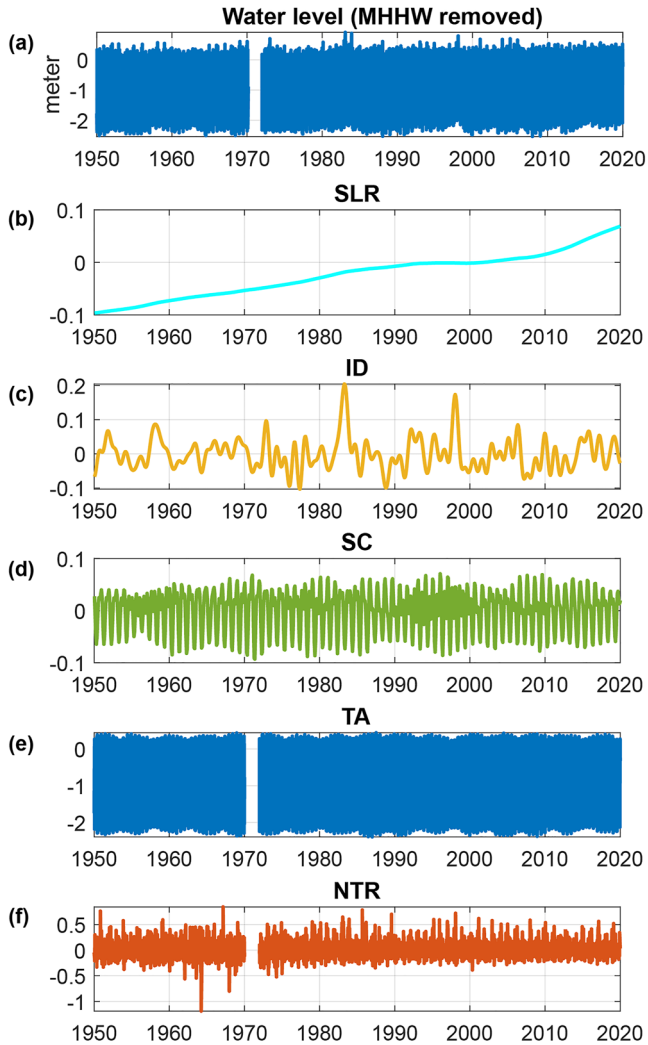

Figure 2. Hourly water level decomposition in San Francisco (in meters). The sea-level rise (SLR) before 1990 is negative as we use the average sea level over the National Tidal Datum Epoch of 1983–2001 as base sea level. Data gaps in tidal anomaly (TA) and Non-tidal residual (NTR) come from missing values in hourly sea level records preventing a robust tidal analysis.

We exclude SLR from this part of the analysis and apply phase scrambling to the other four components (ID, SC, TA, and NTR) to explore whether systematic positive or negative compounding effects exist due to positive or negative correlation between the components. After the phase scrambling, we re-combine the four components and calculate the differences in HTF days per year between the original and the phase-scrambled data. This is repeated 1,000 times at each tide gauge, and we show the median results along with the 25th and 75th percentile values.

4. Results

4.1. Contribution of Different Sea-Level Components to Still Water Levels Causing HTF

An example of the results from the time series analysis at the tide gauge of San Francisco is shown in Figure 2; we focus the analysis on the common period from 1950 to 2019 because very few HTF events occurred before 1950 and fewer tide gauge records are available when going back further in time. SLR in San Francisco since 1950 was ~0.12 m, with a period of relatively low rates of rise in the 1990s and early 2000s and high rates since 2010 (Figure 2b)—driven, in part, by the Pacific Decadal Oscillation which caused broad-scale changes in the North Pacific eastern boundary ocean circulation, affecting upwelling along the eastern boundary and suppressing the rate of SLR (Bromirski et al., 2011). ID has a range of up to 0.3 m (difference between high peaks and low peaks), with two maxima around 1983 and 1998 and a minimum in 1989 (Figure 2c); these extreme events were largely linked to El Niño-Southern Oscillation (ENSO). The amplitudes of SC range from 0.04 to 0.08 m, including, for example, a high amplitude (~0.08 m) around 1969 that was twice as large as the minimum in 2004 (~0.04 m) (Figure 2d). TA is defined here as the predicted tide relative to MHHW; in San Francisco it has a range of ~2.2 m and exhibits a 4.4 year cycle associated with the perigean tide (Figure 2e). NTR at San Francisco shows values from ~-1.0 m (in 1964, as a result of a Tsunami triggered in Alaska (Dengler & Magoon, 2005)) to ~0.75 m (Figure 2f), where high positive values are typically connected to extreme weather events including landfalling atmospheric rivers (e.g., Piecuch et al., 2022). Note that gaps in the TA and NTR components can arise due to insufficient hourly data (i.e., years with less than 75% completeness) to perform the tidal analysis; monthly and annual MSL values are often still available and hence the other components are not always affected. The same data as shown in Figure 2 is produced for all 120 tide gauges around the U.S. with records longer than 20 years.

Using this new database, we identify all HTF hours since 1950, whereas HTF is defined as still water level exceedances of the minor flooding thresholds. The latter is obtained from Sweet et al. (2018) and inferred from a regression analysis using local tidal characteristics if no official minor flooding threshold exists (see Data section). We define the ratio of one sea-level component to the sum of the absolute values of all components as its relative contribution to the still water level anomaly causing HTF. For example, assuming an HTF threshold of 0.4 m above MHHW, if still water level reaches 0.5 m above MHHW and is comprised of 0.7 NTR and −0.2 m TA (indicating that the tidal prediction was below MHHW during the HTF event), NTR would get assigned 78% (0.7/0.9 = 0.78) contribution and TA -22% (−0.2/0.9 = −0.22) contribution. We prefer this approach because individual contributions are less than 100% but absolute contributions add up to 100%. An alternative way would be to allow individual components to contribute more than 100%. Using the same example as before, NTR would then get assigned 140% (0.7/0.4 = 140%) and TA -40% (−0.2/0.5 = −40%). However, the overall conclusions in terms of the relative importance of different components remains the same for both methods (compare Figure 3 and Figure S2 in Supporting Information S1).

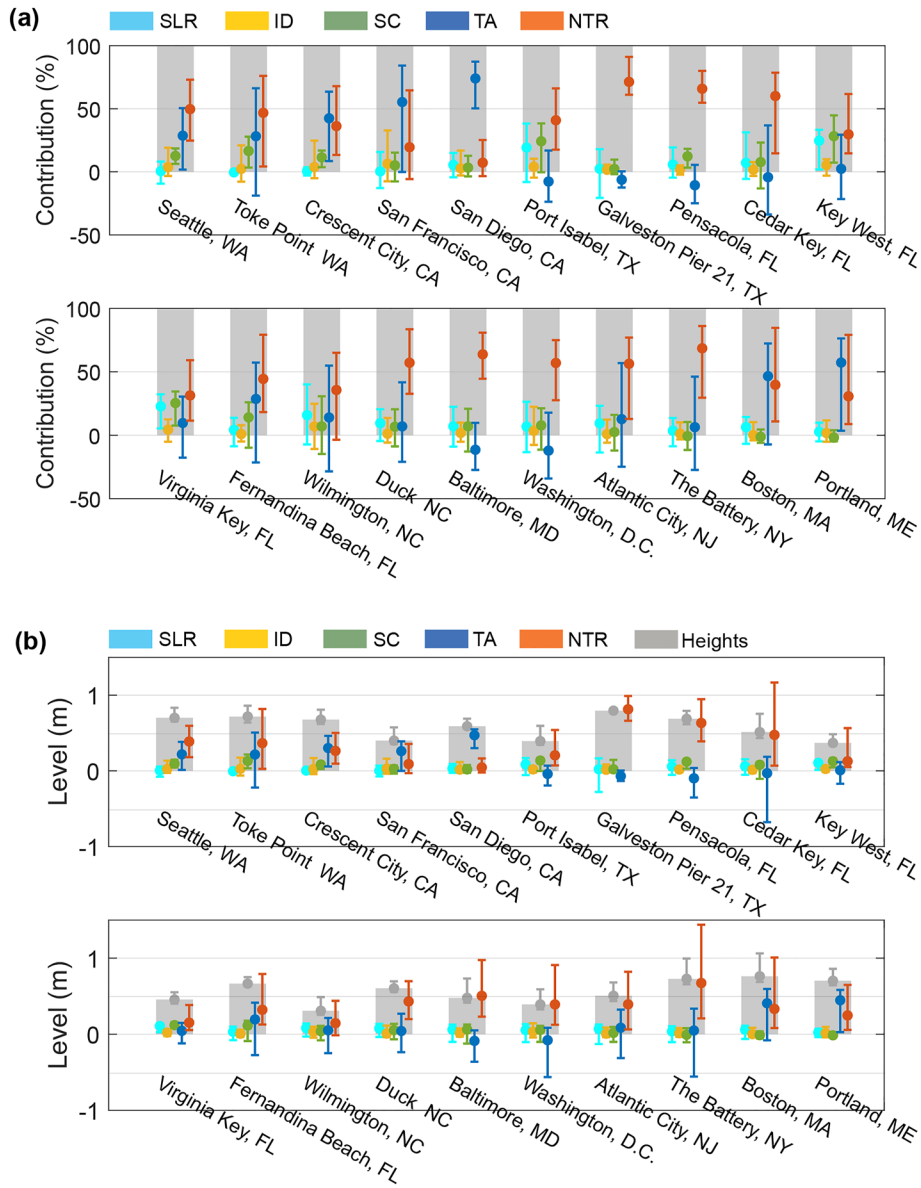

Figure 3. Contributions of different sea-level components to still water levels during high-tide flooding (HTF) between 1950 and 2019 expressed in percent (a) and meters (b). Colored vertical bars represent 5th–95th percentiles of the distribution while filled circles represent the median. Color denotes different components: sea-level rise (SLR) (cyan), interannual-to-decadal (ID) (orange), seasonal cycle (SC) (green), tidal anomaly (TA) (blue), and Non-tidal residual (NTR) (red). The gray bars in (b) denote median water level elevations during HTF relative to Mean Higher High Water. Relative ordering of the sites follows the contiguous U.S. coastline in a counterclockwise sense, starting in the northwest and ending in the northeast. See in Supporting Information S1 for median results at more locations.

Figure 3 shows the results for 20 representative sites, including the median and the 5th to 95th percentile range of the distribution for all HTF hours since 1950 (see Figure S3 in Supporting Information S1 for the median results for other stations). As an example, San Francisco has experienced 593 HTF hr since 1950 and TA was the dominant component for most of those, contributing between 0% and 83% (median is 55%) to the still water level anomaly, or, in absolute values, 0–0.39 m (median is 0.26 m). This is followed by NTR, contributing between −6% and 64% (median is 20%), or −0.03–0.36 m (median is 0.09 m) to still water levels leading to HTF. In contrast, still water levels during HTF at The Battery, NY, are dominated by NTR, contributing between 30% and 85% (median is 68%), or 0.21–1.43 m (median is 0.67 m). Meanwhile, the TA contribution can include negative values when the predicted tide level at the time of HTF was below MHHW; TA values at The Battery range from

−27% to 46% (median is 6%), or −0.56–0.33 m (median is 0.05 m). The contributions (median and spread) of SC and ID are smaller than NTR across all sites and smaller than TA at most sites (exceptions are locations with small tidal ranges), but they can each still contribute 20%–30% to still water levels during individual HTF events. Quantifying the contribution of SLR to still water levels during individual HTF events is inherently ambiguous and unavoidably requires selecting a reference period. Here we chose the National Tidal Datum Epoch of 1983–2001, which means that HTF that happened early in the record (before the base period) get assigned negative SLR contributions. Overall, and partly because of the selection of this base period, the SLR contribution to individual HTF hours is relatively smaller compared to other components.

Next, we can identify large-scale spatial structures across sites in the median contributions of the different sea-level components to HTF (Figure S3 in Supporting Information S1). Along the northeast coast of the U.S., including the Gulf of Maine, TA dominates still water levels during HTF with median contributions of 46%–82% across sites. Further south, NTR becomes most important; for example, the NTR contribution reaches 82% at tide gauges in the New London area and up to 67% at tide gauges in the New York City area. The TA contribution is ∼−15% along the mid-Atlantic coast (between Atlantic City, NJ and Oregon Inlet Marina, NC) and increases to ∼30% along the southeast coast. In contrast, the NTR contribution is 60% along the mid-Atlantic coast but decreases to ∼35% along the southeast coast. The SC becomes more important in the south, contributing 5%–29% along the southeast coast and 5%–26% in the Gulf of Mexico, where it is the second most important component after NTR. On the west coast, however, TA is the dominant component in the south and its relative contribution decreases northward from ∼75% to ∼35%, where NTR (increase from ∼10% in the south to ∼50% in the north) and SC (increase from ∼5% to ∼15%) become more relevant. In the U.S. Pacific islands, NTR is the dominant component (at most locations >70%) while the other four components make relatively small contributions (<10%). ID generally contributes very little compared to other components, and that is because positive and negative contributions cancel each other out when averaging over long time periods. For individual HTF events the ID contribution can be much larger (up to ∼30%), often related to strong ENSO events. As outlined above, SLR is referred to the 1983–2001 tidal epoch, leading to both negative and positive contributions that cancel each other out when averaged over the full analysis period.

4.2. Minimum Number of Sea-Level Components Required to Cause HTF

In the previous section we focused on the relative contribution of each sea-level component to still water level anomalies during HTF. Next, we determine the importance of any given component by analyzing how many sea-level components need to superimpose on the SLR component to exceed HTF thresholds and how their numbers change over time. In the counting process, components with the largest contribution are counted first. For each HTF hour this process is intended to identify the minimum number of components required to cross the threshold (see Methods for more details). We also assess the relationship between the total number of HTF hours and the individual sea-level components and their combinations. In San Francisco, for example, the number of required components to superimpose on SLR declines from two to four components in the 1950s and 1960s to one–three components after 2000 (Figure 4a). As a result, a large portion of HTF hours over the last decade could have been caused by just one sea-level component superimposed on SLR, whereas before combinations of multiple components were required. Figure 4c shows that in San Francisco TA is the component that could have most often caused HTF by itself, especially over the last few decades, due to SLR and increases in tidal range at this location [16]. For instance, TA alone could have resulted in ∼15 HTF hr in 2016 and 2017 and 20 hr in 2018. NTR is the only other component that could have led to HTF without the contribution of other components. In 2019, TA alone could have led to ∼3 HTF hr while NTR alone could have led to ∼7 HTF hr. The highest number of HTF hours (8 hr/year on average) could have been caused by the combination of two components, mainly TA and NTR (Figure 4d). Three components could have combined in different ways in the past to create HTF (Figure 4e) with no combination being particularly prevalent; all four components were required infrequently (Figure 4f). The number of HTF hours in San Francisco driven by different combinations of components also changed over time. HTF requiring three and four components (Figure 4b), increased by 16 hr (from 30 to 46 hr) between 1950–1959 and 2010–2019, whereas it increased by 150 hr (from 34 to 184 hr) for HTF where only one–two components were required.

We can use these results to calculate the ratio of the increased HTF hours caused by one–two and three–four components between the 1950s and 2010s. For example, in San Francisco we find an increase of HTF hours

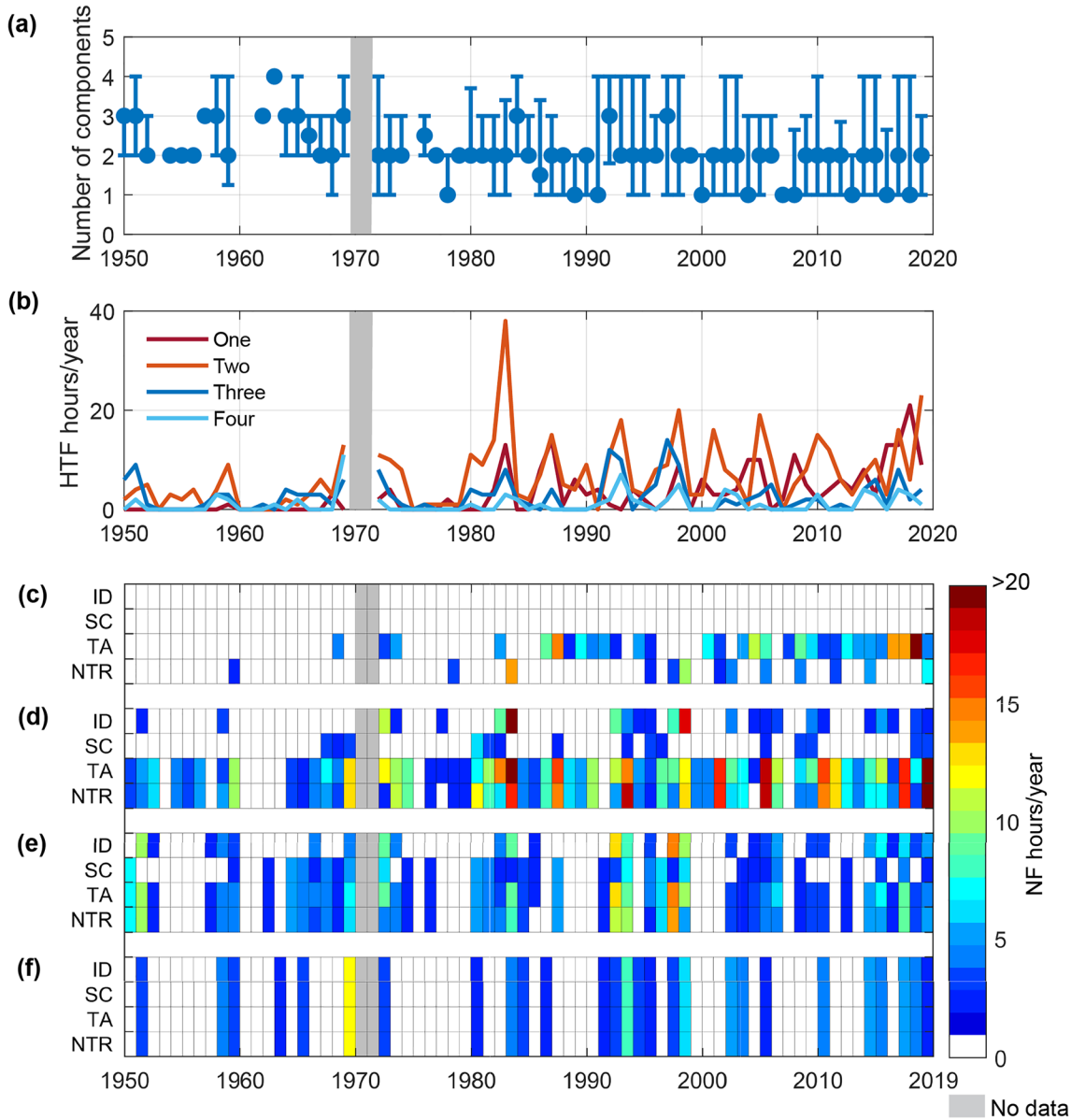

Figure 4. The number of sea-level components required to cause high-tide flooding (HTF). (a) The smallest number of components needed to cross the HTF threshold at San Francisco (see Methods for details on the counting process). Vertical axis denotes the number of components, where error bars represent 5th–95th percentiles (derived from all HTF hours in a year) and filled circles denote the median. Gaps indicate that no HTF occurred in that year. Gray denotes missing or insufficient data to implement the harmonic tidal analysis. (b) HTF hours per year that could have occurred from one, two, three, or four sea-level components. (c–f) similar to (b) but showing which components were involved in HTF hours that could have been caused by one (c), two (d), three (e), and four (f) sea-level component(s).

which only required one and two components of 159 when comparing the 2010–2019 and 1950–1959 aggregated results. For HTF hours that required three–four components we only find an increase of 16. This leads to a ratio is 9.3 (150/16), which means that the increase in HTF hours that could have been caused by one and two components was almost 10 times as rapid as the change in HTF hours that required three and four components. Figure 5 shows the ratio for all locations. When available, we use the 1950–1959 and 2010–2019 periods, but when tide gauge records start later, we use the first 10 years of data instead of 1950–1959. We also tested using 19 year windows to quantify the effect of the nodal cycle; changes in the results were negligible but using such long windows resulted in overlapping periods at many locations where records are relatively short. Overall, the results in Figure 5 indicate that as expected given SLR, many places experienced a more rapid increase in HTF hours caused by one and two components relative to three and four components. The ratios are particularly high

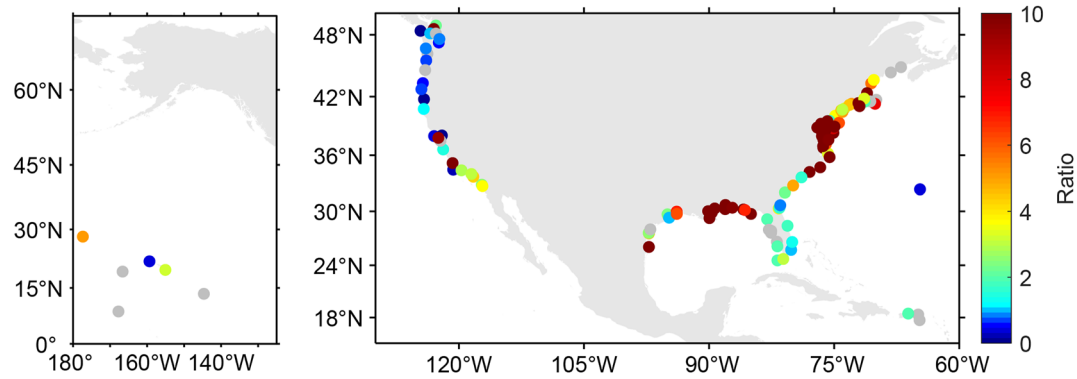

Figure 5. The extent of increased high-tide flooding (HTF) hours by fewer components, expressed as ratios of changes in HTF hours which required one and two components to reach water levels above the flooding thresholds and HTF hours which required three and four components. The changes in HTF hours for both cases were assessed between the 1950s (1950–1959) and 2010s (2010–2019); when records start after 1950, we use the first 10 years of data instead of the 1950–1959 period. Ratios >1 indicate that changes in HTF hours where one and two components were required were relatively larger than changes in four HTF hours where three and components were required; ratios <1 indicate the opposite. Gray circles denote that no HTF occurred during the selected period.

for the northeast, mid-Atlantic, and Gulf of Mexico coastlines. For the southeast coast the ratios are smaller, indicating that changes were more comparable between HTF hours requiring one and two components and those requiring three and four components. In contrast, parts of the northwest coast four had larger changes in HTF hours requiring three and components, as indicated by ratios smaller than 1 (blue color in Figure 5). This is likely a result of smaller or even negative SLR as a result of vertical land motion, among other factors (e.g., Dangendorf et al., 2021).

The analysis presented here highlights that the number of sea-level components required to cause HTF is decreasing due to SLR in most locations along the U.S. coastline. However, it is also clear from these results that in the middle of the 20th century TA alone could not have caused HTF anywhere, and even today, TA alone can only lead to HTF along certain parts of the coast (Figure S4 in Supporting Information S1). In those areas, which include parts of the west coast, northeast, and the South Atlantic Bight, HTF can be solely caused by high tides (e.g., perigean spring tides, or at the peak of the nodal cycle). In nearly all other locations additional sea-level components are required (alone or in combination with TA) to push water levels above HTF thresholds.

4.3. Seasonal Variability of Contributions of Different Sea-Level Components

It is also important from a coastal management perspective to know the time of the year when HTF is likely to occur, and which sea-level components are driving seasonal increases in the frequency of HTF. For the seasonal analysis, we remove the influence of SLR and refer all time series to the base water level derived for the 1983–2001 tidal datum epoch. This can lead to more HTF hours than truly happened, because early parts of the time series are shifted upwards, but it allows us to focus only on the seasonality without the complicating influence of SLR relative to present day conditions.

Detailed results are shown for the San Francisco tide gauge in Figure 6a. This location experienced the highest number of threshold exceedances (after correcting for SLR) in winter (DJF; ~700 hr in total), where ~140 hr were caused by just one component, either TA (in 67% of cases) or NTR (in 33% of cases). The largest amount of ~380 hr was caused by a combination of two components, and TA (92%) and NTR (82%) were most often involved. Only around 50 hr of threshold exceedances in winter required all four components. In spring, when SC is at its lowest, only the other three components contribute to threshold exceedances and hence no HTF occurred that required all four components. Results for summer and fall are similar, with TA being the main component leading to threshold exceedances when only one component was required, and both TA and NTR being involved most often when two or three components were required. These results for San Francisco can be explained by the phases of the seasonal cycles of the different components and the fact that the semi-annual signal in high

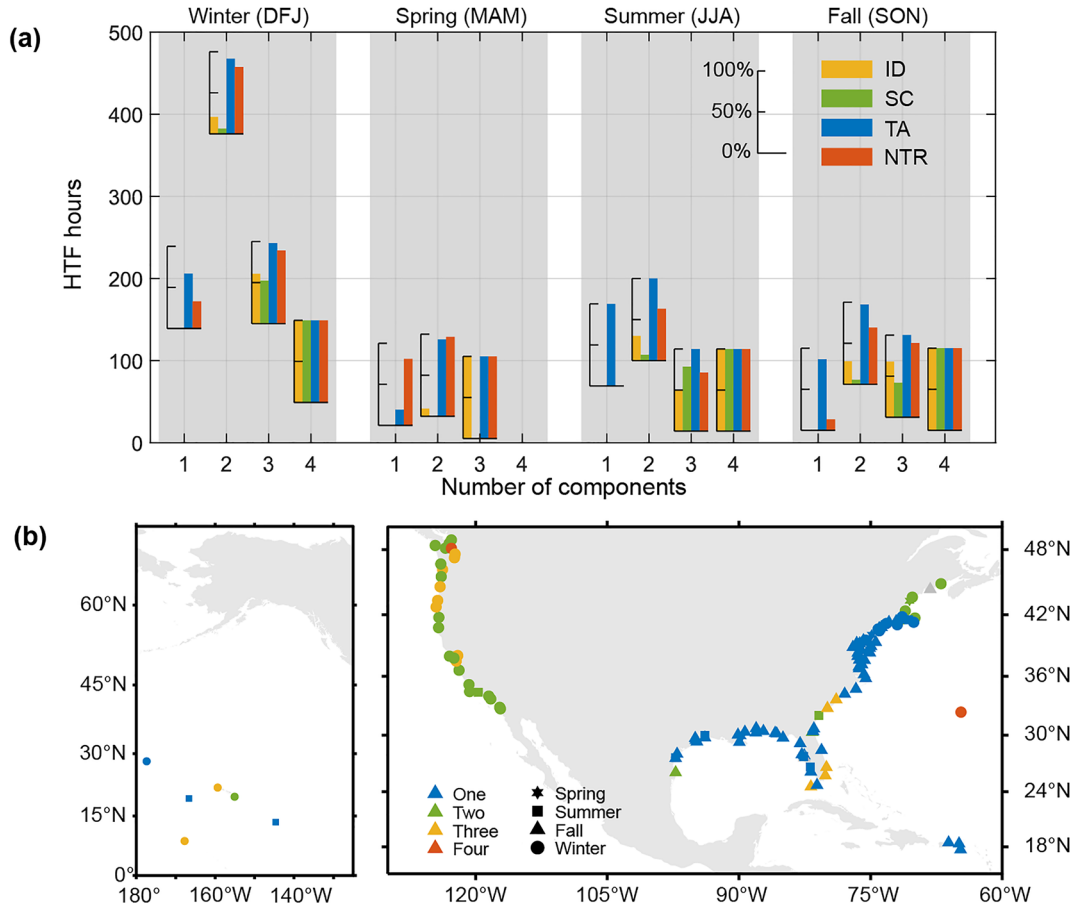

Figure 6. Seasonal features in the number of components needed to create threshold exceedances in (a) San Francisco and (b) the full U.S. coastline. Bar charts in (a) denote the frequencies of components: Interannual-to-decadal (ID) (orange), seasonal cycle (SC) (green), tidal anomaly (TA) (blue), and Non-tidal residual (NTR) (red); x-axis shows the number of components for the four seasons; y-axis shows the sum of exceedance hours caused by the respective number of components in a particular season. The position of the x-axes of the inset bar charts indicates the total amount of exceedance hours for a particular season and number of components. As an example, after removing the influence of sea-level rise, the San Francisco record includes ~380 exceedance hours in winter that required two components. There are six possible combinations (TA + NTR, TA + ID, TA + SC, NTR + SC, NTR + ID and SC + ID) and the summed frequencies of TA, NTR, SC, and ID are 92%, 82%, 6%, and 20%, respectively. (b) The season when the largest amount of exceedance hours occurred (denoted by the marker shape) as well as the number of components that most often led to exceedances in these seasons (denoted by the marker color). San Francisco, for example, experiences the largest number of exceedance hours in winter (see circle marker) and those high-tide flooding (HTF) hours are most often due to the combination of two components (see green color).

tide levels has a larger amplitude than that resulting from the MSL cycle and NTR (see Figure S5 in Supporting Information S1).

Extending the same analysis to the entire U.S. coast, we find that the east and west coasts show distinct seasonal patterns: most HTF hours along the east coast occur in fall (locations indicated by triangles), while winter is the most active HTF season for the west coast (locations indicated by circles) (Figure 6b). The number of components required for HTF during the peak winter season on the west coast increases from two in the southern part (indicated by the green color) to three or four components in the northern part (indicated by the orange and red). In the Gulf of Mexico and mid-Atlantic coast most HTF hours during the peak fall season are caused by only one component, in this case NTR. In the South Atlantic Bight, HTF also mostly occurs in fall, however HTF hours are most often associated with three components during this season. Along the northeast coast more HTF occurs in winter and two components are most often involved, particularly at the northernmost stations. For the Pacific islands there is no coherent seasonal patterns with the HTF peaks happening in different seasons.

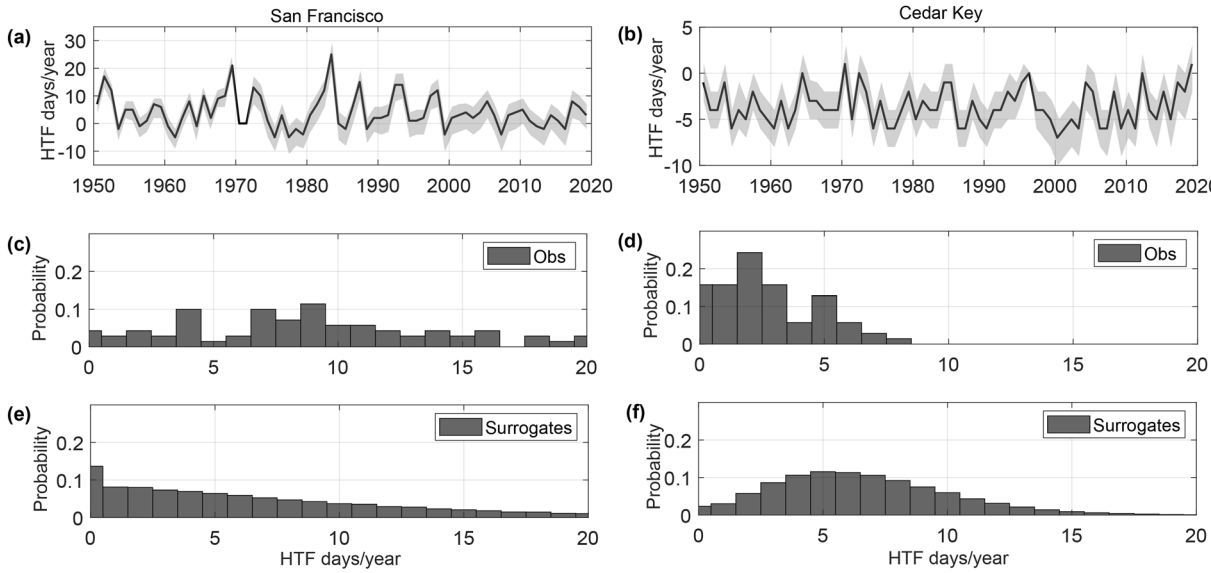

Figure 7. Difference of high-tide flooding (HTF) days per year from comparing original and phase-scrambled (seasonal cycle, interannual-to-decadal, tidal anomaly, and non-tidal residual) time series at (a) San Francisco and (b) Cedar Key after creating 1,000 phase-scrambled surrogates for each component; results are shown for the 50th percentiles and shaded bands represent 25th and 75th levels. Positive values indicate the existence of positive correlation between sea-level components and negative value indicate existence of negative correlation. (c–f) histograms of the threshold exceedance days derived from observations (c and d) and 1,000 surrogate time series (e and f).

4.4. Compounding Effects Due To Co-Variability in Sea-Level Components

Finally, we explore compounding effects due to co-variability between sea-level component contributions to HTF. Like the seasonal analysis, we remove the influence of SLR and focus on the other four components. We apply phase scrambling to those components to explore whether there are significant positive or negative compounding effects. After the phase scrambling, we re-combine the four components and quantify differences in the number of threshold exceedance days between the original data (with SLR influence removed) and the phase-scrambled data; this is repeated 1,000 times. In San Francisco, there is a tendency for more exceedances and higher positive values in the original data (Figure 7a), indicating the presence of positive compounding effects, and highlighting the existence of positive co-variability between certain sea-level components. Histograms for the number of exceedance days per year derived from the observations (Figure 7c) and the 1,000 surrogate time series (Figure 7e) also show differences, with the observations showing a higher probability of threshold exceedances.

In contrast, along the east coast, we find that many locations have negative compounding effects, meaning that more HTF days are found in the phase-scrambled data compared to the original data. One example is Cedar Key on the west coast of Florida, where there are consistently less exceedance days in the original data (Figure 7b), indicating the existence of negative compounding effects and thus negative co-variability between different sea-level components. Again, the histograms derived from observations (Figure 7d) and surrogate data (Figure 7f) also show this, with a higher probability of threshold exceedances. This negative co-variability results from the seasonal cycles of the different components being out of phase (Figure S6 in Supporting Information S1). Specifically, TA and SC have their high peaks in relatively close succession (June and August), but at the same time NTR (peaks in January) is at its lowest. Considering the strong regional coherence in SC and NTR, as well as the SC of TA, we would expect to find similar results at other locations close to Cedar Key, such as Fort Myers to the south or Pensacola to the north. However, at those locations we do not find the same negative compounding effects (Figure S7 in Supporting Information S1). This is because the flooding thresholds are different; they are relatively higher than MHHW in Pensacola and Fort Myers as compared to Cedar Key due to greater diurnal ranges. Therefore, threshold exceedances in Pensacola and Fort Myers typically only occur with relatively large NTR values. However, as the gap between the HTF thresholds and MHHW decreases due to SLR, similar negative compounding effects are likely to emerge (Figure S7 in Supporting Information S1).

5. Discussion

Previous studies which assessed the role of different sea level components (or processes) in generating high coastal water levels typically decomposed observed still water levels into three components, namely, tides, NTR, and MSL. Merrifield et al. (2013) further decomposed NTR into high and low frequency components to explore the geographic patterns of their contributions, while Ferrarin et al. (2022) further decomposed NTR into seiches, planetary atmospheric waves, and wave set-up to explore the correlation and compounding effects between sea level components; they also included sea level variability at different time scales in addition to relative SLR. Here we decompose observed still water levels into five components, SLR, ID, SC, TA, and NTR, where the first three are related to MSL changes at different time scales.

Our first objective was to assess the relative contribution of the individual components to HTF at 120 tide gauges since 1950. While we find distinct differences across the U.S. coastline, we also identify strong regional coherence where certain components are most relevant to HTF. Examples are the west coast, where SLR is relatively less important (and less pronounced) and TA is more important (particularly in the southwest); or along the northeast and Gulf coasts where NTR is most relevant. This is in line with previous studies on the role of different sea level components in generating high coastal water levels (e.g., Melet et al., 2018; Merrifield et al., 2013; Serafin et al., 2017; Sweet et al., 2018). The magnitude and contribution of SC to HTF events is largest along the U.S. Gulf coast, which is consistent with the results in Ray et al. (2021) showing larger SC amplitudes in this region.

Our second objective was to assess the number of components that are required to cause HTF and how this has changed over time. We find that the number of components (on top of SLR) required to cause HTF has decreased since 1950, especially along the southwest, east, and Gulf coasts. Particularly TA and NTR, either alone or in combination, can now cause HTF, whereas in the past three or four components were often required. The main reason for this change is SLR, closing the gap between MHHW and HTF thresholds. At the southwest coast, TA (on top of SLR) is the main driver of HTF, but additional components are still needed to push water levels beyond HTF thresholds. In the Gulf of Mexico and mid-Atlantic regions, NTR is the main HTF driver and could alone (without other components) have caused the highest number of HTF hours. HTF induced solely by TA (the only component i.e., predictable) can only occur in few locations under present sea-level conditions but will become more frequent and occur in more places with continuing SLR (Sweet et al., 2018). When assessing ratios that reflect changes in HTF events that required 3–4 versus. 1–2 sea level components we find relatively low values around Florida and along the coasts of Georgia and South Carolina (Figure 5), compared with the other parts of the Gulf and east coast. The reason for this is the differing role of NTR and TA. In places where NTR is dominant, it can alone be enough to create HTF events, and hence SLR greatly increases the number of HTF events requiring one and two components, which in turn leads to high ratios. In places where TA dominates, additional processes are often still required to contribute to exceed the HTF thresholds. The variance of TA along the southeast coast is higher than along the Gulf coast (e.g., Sweet et al., 2018), which means more HTF events are associated with TA and the change in HTF events requiring only one and two components is smaller (leading to smaller ratios). Locations in south Florida (i.e., Key West and Vaca Key) show lower variance in NTR when compared with the northern Gulf coast, but higher variance in SC, which by itself is also not large enough to create HTF events. Thus, the changes in the number of HTF events which require fewer components (and with that the ratios) are also smaller than those along most other parts of the Gulf coast.

Our third objective was to assess the seasonality of HTF and the associated sea level components. Our results confirm that seasonality in HTF along the west coast is dominated by tidal modulations (Sweet et al., 2018), especially the semi-annual cycle. We also find that along the west coast HTF occurs more often during the months adjacent to the winter/summer solstices, in agreement with previous studies (Ray & Merrifield, 2019).

Our last objective was to assess compounding effects resulting from co-variability of different sea-level components. We find that compounding is less pronounced on the east coast compared to the west coast, likely due to the peaks of the seasonal cycles of the different components being out of phase on the east coast, but also due to the larger differences in HTF thresholds relative to MHHW. With SLR closing this gap, east coast locations like Fort Myers and Pensacola will gradually show more compounding effects (Figure S7 in Supporting Information S1). As MHHW nears the HTF threshold, the ID component also becomes more relevant, with the potential to both counteract or exacerbate the frequency of HTF. While not included in our analysis, compounding effects also exist between the sea level components analyzed here and pluvial/fluvial flooding drivers (Bevacqua et al., 2020;

Ghanbari et al., 2021; Nasr et al., 2021; Wahl et al., 2015) and dynamic wave contributions (Marcos et al., 2017; Nasr et al., 2021).

6. Conclusions

We quantify hourly time series of SLR, ID, SC, TA, and NTR and the role of these sea-level components in causing HTF along the U.S. coastline. We identify the spatial distribution and relative importance of different sea level components for the period since 1950, explore how many components need to combine to cause HTF and how it changed over time, assess the role of seasonality in different sea level components and HTF, and finally quantify how compounding effects between different sea level components contribute to HTF.

At this point our study based on tide gauge measurements represents a purely local temporal analysis, but future studies should include a more complete spatiotemporal analysis, also computing contributions from a variety of spatial scales. We also assume in our water level decomposition that sea-level components can be linearly superimposed, whereas in reality, complex non-linear interactions exist. Therefore, removing one component could lead to a response in one or more of the other components. Such interactions are not accounted for here and we defer the quantification of their role to a later study. Finally, we do not account for wave contributions in our analysis which can also contribute, through wave setup, to high total level events (e.g., Melet et al., 2018; Serafin et al., 2017; Vitousek et al., 2017) and hence exceedances of HTF thresholds. Most of the tide gauges are installed in sheltered areas where wave effects are small but it cannot be ruled out that wave effects have contributed to some of the HTF events we identify for the past. Further investigating the role of waves in the context of our analysis, also because of the known correlation between waves and other sea level processes (in particular NTR), is another potential avenue for future research.

To conclude, we derive a new database consisting of hourly time series of five sea-level components, representing different processes, and their changes through time. Analyzing this database provided new insights into the spatiotemporal patterns of the contributions of different sea-level components to HTF and will lay the foundation for a better understanding of the predictability of HTF events.

Conflict of Interest

The authors declare no conflicts of interest relevant to this study.

Data Availability Statement

The data are available at https://tidesandcurrents.noaa/gov/map/index.shtml (hourly water level), https://www.psmsl.org (annual MSL), https://tidesandcurrents.noaa.gov/publications/techrpt86_PaP_of_HTFlooding.pdf (HTF threshold) and https://api.tidesandcurrents.noaa.gov/mdapi/prod/webapi/stations/8447930/floodlevels.json?units=metric by changing "8447930" with other station ID. The data base of the time-varying sea level components used for the analysis is publicly available at Figshare via https://doi.org/10.6084/m9.figshare.16825540.v1 or direct link https://figshare.com/articles/dataset/Sea_level_components_and_contribution/16825540 with license CC BY 4.0. Matlab code used for the database development and analysis can be found at Github: https://github.com/CoRE-Lab-UCF/Sea-level-components-and-contribution.

Acknowledgments
The authors declare no competing interests. This work was supported by NASA's Sea Level Change Team award number 80NSSC20K1241. S.L. also acknowledges support by the China Scholarship Council (no. 201904910413) and the Ministry of Science and Technology of the People's Republic of China (grant no. 2011YQ120045).

References

Bevacqua, E., Vousdoukas, M. I., Zappa, G., Hodges, K., Shepherd, T. G., Maraun, D., et al. (2020). More meteorological events that drive compound coastal flooding are projected under climate change. *Communications earth & environment*, *1*(1), 47. https://doi.org/10.1038/s43247-020-00044-z

Bromirski, P. D., Miller, A. J., Flick, R. E., & Auad, G. (2011). Dynamical suppression of sea level rise along the Pacific coast of North America: Indications for imminent acceleration. *Journal of Geophysical Research*, *116*, 2010JC006759. https://doi.org/10.1029/2010JC006759

Calafat, F. M., Chambers, D. P., & Tsimplis, M. N. (2012). Mechanisms of decadal sea level variability in the eastern North Atlantic and the Mediterranean Sea. *Journal of Geophysical Research*, *117*(C9). https://doi.org/10.1029/2012jc008285

Calafat, F. M., Wahl, T., Lindsten, F., Williams, J., & Frajka-Williams, E. (2018). Coherent modulation of the sea-level annual cycle in the United States by Atlantic Rossby waves. *Nature Communications*, *9*(1), 2571. https://doi.org/10.1038/s41467-018-04898-y

Chambers, D. P., Merrifield, M. A., & Nerem, R. S. (2012). Is there a 60-year oscillation in global mean sea level? *Geophysical Research Letters*, *39*(18), L18607. https://doi.org/10.1029/2012gl052885

Cherqui, F., Belmeziti, A., Granger, D., Sourdril, A., & Le Gauffre, P. (2015). Assessing urban potential flooding risk and identifying effective risk-reduction measures. *Science of the Total Environment*, *514*, 418–425. https://doi.org/10.1016/j.scitotenv.2015.02.027

Codiga, D. (2011). *Unified tidal analysis and prediction using the UTide Matlab functions*. Graduate School of Oceanography. https://doi.org/10.13140/RG.2.1.3761.2008

Dahl, K. A., Fitzpatrick, M. F., & Spanger-Siegfried, E. (2017). Sea level rise drives increased tidal flooding frequency at tide gauges along the U.S. East and Gulf Coasts: Projections for 2030 and 2045. *PLoS One*, *12*(2), e0170949. https://doi.org/10.1371/journal.pone.0170949

Dangendorf, S., Calafat, F. M., Arns, A., Wahl, T., Haigh, I. D., & Jensen, J. (2014). Mean sea level variability in the North Sea: Processes and implications. *Journal of Geophysical Research: Oceans*, *119*, 6820–6841. https://doi.org/10.1002/2014jc009901

Dangendorf, S., Frederikse, T., Chafik, L., Klinck, J. M., Ezer, T., & Hamlington, B. D. (2021). Data-driven reconstruction reveals large-scale ocean circulation control on coastal sea level. *Nature Climate Change*, *11*(6), 514–520. https://doi.org/10.1038/s41558-021-01046-1

Dangendorf, S., Marcos, M., Wöppelmann, G., Conrad, C. P., Frederikse, T., & Riva, R. (2017). Reassessment of 20th century global mean sea level rise. *Proceedings of the National Academy of Sciences*, *114*(23), 5946–5951. https://doi.org/10.1073/pnas.1616007114

Daubechies, I. (1992). *Ten lectures on wavelets*. Society for Industrial and Applied Mathematics.

Dengler, L. A., & Magoon, O. (2005). The 1964 Tsunami in Crescent city, California: A 40-year retrospective. In *Solutions to coastal disasters 2005* (pp. 639–648). https://doi.org/10.1061/40774(176)64

Ezer, T. (2019). Analysis of the changing patterns of seasonal flooding along the U.S. East Coast. *Ocean Dynamics*, *70*(2), 241–255. https://doi.org/10.1007/s10236-019-01326-7

Ferrarin, C., Lionello, P., Orlic, M., Raicich, F., & Salvadori, G. (2022). Venice as a paradigm of coastal flooding under multiple compound drivers. *Scientific Reports*, *12*(1), 5754. https://doi.org/10.1038/s41598-022-09652-5

Fox, J., & Weisberg, S. (2011). *An R companion to applied regression*. Sage. Retrieved from https://socialsciences.mcmaster.ca/jfox/Books/Companion-2E/appendix/Appendix-Robust-Regression.pdf

Ghanbari, M., Arabi, M., Kao, S. C., Obeysekera, J., & Sweet, W. (2021). Climate change and changes in compound coastal-riverine flooding hazard along the U.S. Coasts. *Earth's Future*, *9*(5). https://doi.org/10.1029/2021ef002055

Hague, B. S., Jones, D. A., Jakob, D., McGregor, S., & Reef, R. (2022). Australian coastal flooding trends and forcing factors. *Earth's Future*, *10*(2), e2021EF002483. https://doi.org/10.1029/2021ef002483

Hino, M., Belanger, S. T., Field, C. B., Davies, A. R., & Mach, K. J. (2019). High-tide flooding disrupts local economic activity. *Science Advances*, *5*(2), eaau2736. https://doi.org/10.1126/sciadv.aau2736

Huber, P. J. (1981). *Robust statistics*. John Wiley & Sons.

Kulp, S. A., & Strauss, B. H. (2019). New elevation data triple estimates of global vulnerability to sea-level rise and coastal flooding. *Nature Communications*, *10*(1), 4844. https://doi.org/10.1038/s41467-019-12808-z

Li, S., Wahl, T., Talke, S. A., Jay, D. A., Orton, P. M., Liang, X., et al. (2021). Evolving tides aggravate nuisance flooding along the U.S. coastline. *Science Advances*, *7*(10), eabe2412. https://doi.org/10.1126/sciadv.abe2412

Losada, I., Reguero, B., Méndez, F., Castanedo, S., Abascal, A., & Mínguez, R. (2013). Long-term changes in sea-level components in Latin America and the Caribbean. *Global and Planetary Change*, *104*, 34–50. https://doi.org/10.1016/j.gloplacha.2013.02.006

Lowe, R. J., Cuttler, M. V. W., & Hansen, J. E. (2021). Climatic drivers of extreme sea level events along the coastline of Western Australia. *Earth's Future*, *9*(4), e2020EF001620. https://doi.org/10.1029/2020ef001620

Marcos, M., Marzeion, B., Dangendorf, S., Slangen, A. B. A., Palanisamy, H., & Fenoglio-Marc, L. (2017). Internal variability versus anthropogenic forcing on sea level and its components. *Surveys in Geophysics*, *38*(1), 329–348. https://doi.org/10.1007/s10712-016-9373-3

Melet, A., Meyssignac, B., Almar, R., & Le Cozannet, G. (2018). Under-estimated wave contribution to coastal sea-level rise. *Nature Climate Change*, *8*(3), 234–239. https://doi.org/10.1038/s41558-018-0088-y

Merrifield, M. A., Genz, A. S., Kontoes, C. P., & Marra, J. J. (2013). Annual maximum water levels from tide gauges: Contributing factors and geographic patterns. *Journal of Geophysical Research: Oceans*, *118*(5), 2535–2546. https://doi.org/10.1002/jgrc.20173

Moftakhari, H. R., AghaKouchak, A., Sanders, B. F., Feldman, D. L., Sweet, W., Matthew, R. A., & Luke, A. (2015). Increased nuisance flooding along the coasts of the United States due to sea level rise: Past and future. *Geophysical Research Letters*, *42*(22), 9846–9852. https://doi.org/10.1002/2015gl066072

Moftakhari, H. R., AghaKouchak, A., Sanders, B. F., & Matthew, R. A. (2017). Cumulative hazard: The case of nuisance flooding. *Earth's Future*, *5*(2), 214–223. https://doi.org/10.1002/2016ef000494

Nasr, A. A., Wahl, T., Rashid, M. M., Camus, P., & Haigh, I. D. (2021). Assessing the dependence structure between oceanographic, fluvial, and pluvial flooding drivers along the United States coastline. *Hydrology and Earth System Sciences*, *25*(12), 6203–6222. https://doi.org/10.5194/hess-25-6203-2021

Pawlowicz, R., Beardsley, B., & Lentz, S. (2002). Classical tidal harmonic analysis including error estimates in MATLAB using T_TIDE. *Computers & Geosciences*, *28*(8), 929–937. https://doi.org/10.1016/S0098-3004(02)00013-4

Piecuch, C. G., Coats, S., Dangendorf, S., Landerer, F. W., Reager, J. T., Thompson, P. R., & Wahl, T. (2022). High-tide floods and storm surges during atmospheric rivers on the US West Coast. *Geophysical Research Letters*, *49*(2), e2021GL096820. https://doi.org/10.1029/2021GL096820

Prichard, D., & Theiler, J. (1994). Generating surrogate data for time series with several simultaneously measured variables. *Physical Review Letters*, *73*(7), 951–954. https://doi.org/10.1103/PhysRevLett.73.951

Pugh, D., & Woodworth, P. (2014). *Sea-level science: Understanding tides, surges, tsunamis and mean sea level changes*. Cambridge University Press.

Rashid, M. M., Wahl, T., Chambers, D. P., Calafat, F. M., & Sweet, W. V. (2019). An extreme sea level indicator for the contiguous United States coastline. *Scientific Data*, *6*(1), 326. https://doi.org/10.1038/s41597-019-0333-x

Ray, R. D., & Foster, G. (2016). Future nuisance flooding at Boston caused by astronomical tides alone. *Earth's Future*, *4*(12), 578–587. https://doi.org/10.1002/2016EF000423

Ray, R. D., Loomis, B. D., & Zlotnicki, V. (2021). The mean seasonal cycle in relative sea level from satellite altimetry and gravimetry. *Journal of Geodesy*, *95*(7), 80. https://doi.org/10.1007/s00190-021-01529-1

Ray, R. D., & Merrifield, M. (2019). The semiannual and 4.4-year modulations of extreme high tides. *Journal of Geophysical Research: Oceans*, *124*(8), 5907–5922. https://doi.org/10.1029/2019JC015061

Rueda, A., Vitousek, S., Camus, P., Tomás, A., Espejo, A., Losada, I. J., et al. (2017). A global classification of coastal flood hazard climates associated with large-scale oceanographic forcing. *Scientific Reports*, *7*(1), 1–8. https://doi.org/10.1038/s41598-017-05090-w

Serafin, K. A., Ruggiero, P., & Stockdon, H. F. (2017). The relative contribution of waves, tides, and nontidal residuals to extreme total water levels on U.S. West Coast sandy beaches. *Geophysical Research Letters*, *44*(4), 1839–1847. https://doi.org/10.1002/2016gl071020

Sweet, W. V., Dusek, G., Obeysekera, J., & Marra, J. J. (2018). *Patterns and projections of high tide flooding along the U.S. coastline using a common impact threshold*. Tech. Rep., NOAA NOS CO-OPS 086, 2018. Retrieved from https://tidesandcurrents.noaa.gov/publications/techrpt86_PaP_of_HTFlooding.pdf

Sweet, W. V., & Park, J. (2014). From the extreme to the mean: Acceleration and tipping points of coastal inundation from sea level rise. *Earth's Future*, *2*(12), 579–600. https://doi.org/10.1002/2014ef000272

Taherkhani, M., Vitousek, S., Barnard, P. L., Frazer, N., Anderson, T. R., & Fletcher, C. H. (2020). Sea-level rise exponentially increases coastal flood frequency. *Scientific Reports*, *10*(1), 6466. https://doi.org/10.1038/s41598-020-62188-4

The MathWorks, I. (2021b). *Wavelet-packets, Natick, Massachusetts, United state*. Retrieved from https://www.mathworks.com/help/wavelet/ug/wavelet-packets.html

Thompson, P. R., Widlansky, M. J., Hamlington, B. D., Merrifield, M. A., Marra, J. J., Mitchum, G. T., & Sweet, W. (2021). Rapid increases and extreme months in projections of United States high-tide flooding. *Nature Climate Change*, *11*(7), 584–590. https://doi.org/10.1038/s41558-021-01077-8

Thompson, P. R., Widlansky, M. J., Merrifield, M. A., Becker, J. M., & Marra, J. J. (2019). A statistical model for frequency of coastal flooding in Honolulu, Hawaii, during the 21st century. *Journal of Geophysical Research: Oceans*, *124*(4), 2787–2802. https://doi.org/10.1029/2018jc014741

Vitousek, S., Barnard, P. L., Fletcher, C. H., Frazer, N., Erikson, L., & Storlazzi, C. D. (2017). Doubling of coastal flooding frequency within decades due to sea-level rise. *Scientific Reports*, *7*(1), 1399. https://doi.org/10.1038/s41598-017-01362-7

Vousdoukas, M. I., Mentaschi, L., Voukouvalas, E., Verlaan, M., & Feyen, L. (2017). Extreme sea levels on the rise along Europe's coasts. *Earth's Future*, *5*(3), 304–323. https://doi.org/10.1002/2016EF000505

Wahl, T., Calafat, F. M., & Luther, M. E. (2014). Rapid changes in the seasonal sea level cycle along the US Gulf coast from the late 20th century. *Geophysical Research Letters*, *41*(2), 491–498. https://doi.org/10.1002/2013gl058777

Wahl, T., & Chambers, D. P. (2015). Evidence for multidecadal variability in US extreme sea level records. *Journal of Geophysical Research: Oceans*, *120*(3), 1527–1544. https://doi.org/10.1002/2014jc010443

Wahl, T., Haigh, I. D., Woodworth, P. L., Albrecht, F., Dillingh, D., Jensen, J., et al. (2013). Observed mean sea level changes around the North Sea coastline from 1800 to present. *Earth-Science Reviews*, *124*, 51–67. https://doi.org/10.1016/j.earscirev.2013.05.003

Wahl, T., Jain, S., Bender, J., Meyers, S. D., & Luther, M. E. (2015). Increasing risk of compound flooding from storm surge and rainfall for major US cities. *Nature Climate Change*, *5*(12), 1093–1097. https://doi.org/10.1038/nclimate2736